A High-Power InP Resonant Tunnelling Diode Heterostructure for 300-GHz Oscillator Sources

Davide Cimbri[#1], Razvan Morariu[#], Afesomeh Ofiare[#], and Edward Wasige[#]

[#]High-Frequency Electronics group, Division of Electronics and Nanoscale Engineering,
James Watt School of Engineering, University of Glasgow, G12 8LT, Glasgow, United Kingdom

[1]davide.cimbri@glasgow.ac.uk

***Abstract*— A high-power double-barrier resonant tunnelling diode (RTD) epitaxial structure in InP technology is reported. The heterostructure exhibits moderate available current density $\Delta J \simeq 1.4$ mA/μm^2 and large voltage swing $\Delta V \simeq 1.2$ V, resulting in a maximum RF power $P_{RF,max} \simeq 0.31$ mW/μm^2, and over 530 GHz bandwidth, being 25 μm^2, 36 μm^2, and 49 μm^2 large RTD devices expected to deliver up to 5 mW, 7 mW, and 10 mW at 300 GHz, respectively. Distributed inductors in both coplanar and microstrip geometry are designed through full 3D electromagnetic simulations, proving the feasibility of the proposed approach for the practical realisation of high-power 300-GHz oscillator sources employing low-cost optical lithography.**

***Keywords*— Indium phosphide, resonant tunnelling diode, double-barrier quantum well, heterostructure, low-terahertz oscillator, RF stub.**

I. Introduction

The resonant tunnelling diode (RTD) is among the main room temperature (RT) semiconductor candidate devices which will allow terahertz (THz) technology to be employed in practical application scenarios, including high-speed wireless data links [1] and high-resolution imaging and spectroscopic apparatuses [2]. Currently, RTD-based low-THz ($\sim 100-300$ GHz) emitters suffer from low output power operation caused by the poor epitaxial structure design and wafer crystal quality, being ~ 1 mW the highest value ever reported for a single indium phosphide (InP) RTD device around 300 GHz [3].

In this paper, we report about an InP RTD heterostructure that features high-power capabilities in the 300-GHz band. The epitaxial structure was designed to achieve several milliwatts (mW) of RF power and then experimentally investigated. To prove the practical employability of RTD devices in real oscillator circuits, both coplanar waveguide (CPW) and microstrip inductive stubs are designed by means of a complete 3D electromagnetic simulation analysis.

II. RTD Heterostructure

The proposed *n*-type intraband epitaxial structure consists of an indium gallium arsenide/aluminium arsenide ($In_{0.53}Ga_{0.47}As$/AlAs) double-barrier quantum well (DBQW) structure featuring moderately-thick AlAs barriers ($\simeq 1.46$ nm) and $In_{0.53}Ga_{0.47}As$ QW ($\simeq 4.39$ nm), asymmetric spacers, and heavily-doped emitter/collector contacts ($N_D = 5 \times 10^{19}$ cm^{-3}), grown on top and lattice-matched to a semi-insulating (SI) InP substrate, which was designed through a non-equilibrium Green's function (NEGF)-based quantum transport simulation tool [4] to achieve moderate peak current density $J_p \sim 2$ mA/μm^2 and large voltage swing $\Delta V > 1$ V [5]. The heterostructure was then investigated through the microfabrication and characterisation of RTD devices. A scanning electron microscopy (SEM) image of a fabricated device with top mesa area $A \simeq 5.5$ μm^2 is shown in Fig. 1. Details of the fabrication process were reported elsewhere [4], while the electrical characteristics and high-frequency RF power performance of the proposed wafer epi-stack are reported in Table 1. Due to the instability of the measured devices, direct S-parameters measurement in the negative differential resistance (NDR) region was not feasible and the capacitance C_{rtd} was retrieved through the extracted QW-to-collector electron escape rate ν_c (assumed bias-independent) in the positive differential resistance (PDR) regions by modelling the negative differential conductance (NDC) $-G_{rtd}(V)$ through a 6th-order polynomial. The measured current-voltage (IV) characteristic, as well as modelled NDC, and associated C_{rtd} and negative QW inductance $-L_{qw}$, are reported in Fig. 2, while an example of fitting of S_{11} and converted Z_{11} parameters at $V = 0.3$ V for the extraction of ν_c is reported in Fig. 3. To do that, a simple small-signal equivalent circuit model of the RTD device, including the parasitic series resistance R_s,

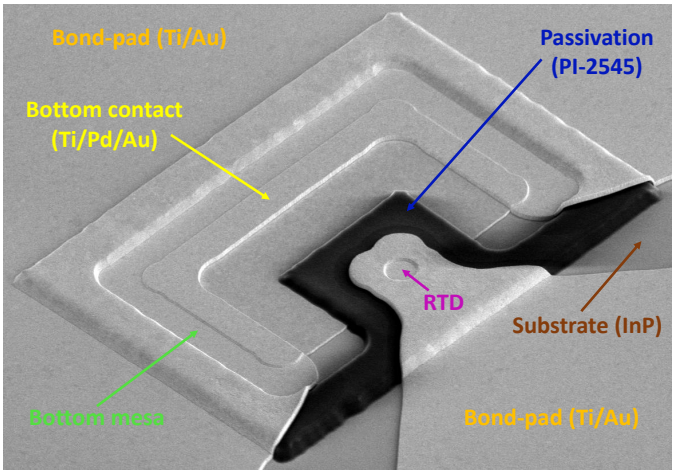

Fig. 1. SEM image of a fabricated $\simeq 5.5$ μm^2 large RTD. The device was passivated using polyimide PI-2545, Ohmic contacts were fabricated employing titanium/palladium/gold (Ti/Pd/Au) metals stacks, while bond-pads consisted of thin Ti/Au layers.

Table 1. RTD heterostructure electrical properties and RF power performance.

ΔJ [mA/μm^2]	ΔV [V]	$-G^*_{rtd}$ [mS/μm^2]	C^*_{rtd} [fF/μm^2]
1.38	1.2	-3.0	5.85
τ_i^{**} [ps]	f_i^{**} [THz]	$P_{RF,max}$	P_{RF} (300 GHz)
0.33	0.77	0.31 mW/μm^2	0.26 mW/μm^2
ρ_c [Ω μm^2]	f_{max} [GHz]	f_c [GHz]	P_{RF} (300 GHz)
4	741	534	0.20 mW/μm^2

In the above, ΔJ is the available current density, τ_i and f_i are the intrinsic delay time and intrinsic cut-off frequency limit, respectively, $P_{RF,max}$ is the maximum RF power, while f_{max} is the maximum oscillation frequency. * Estimated in the NDR region. ** Estimated from self-consistent Schrödinger-Poisson numerical simulations.

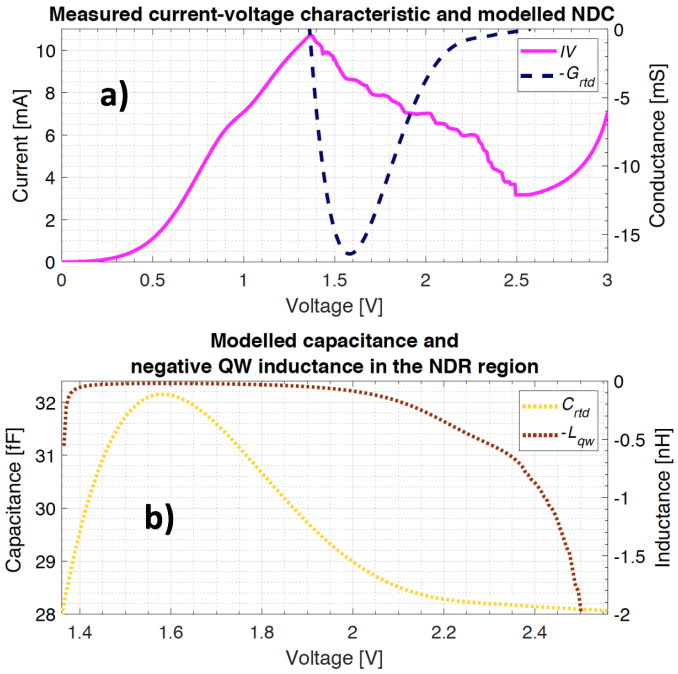

Fig. 2. In a), measured static IV characteristic and modelled NDC, while, in b), modelled capacitance and negative QW inductance in the NDR region.

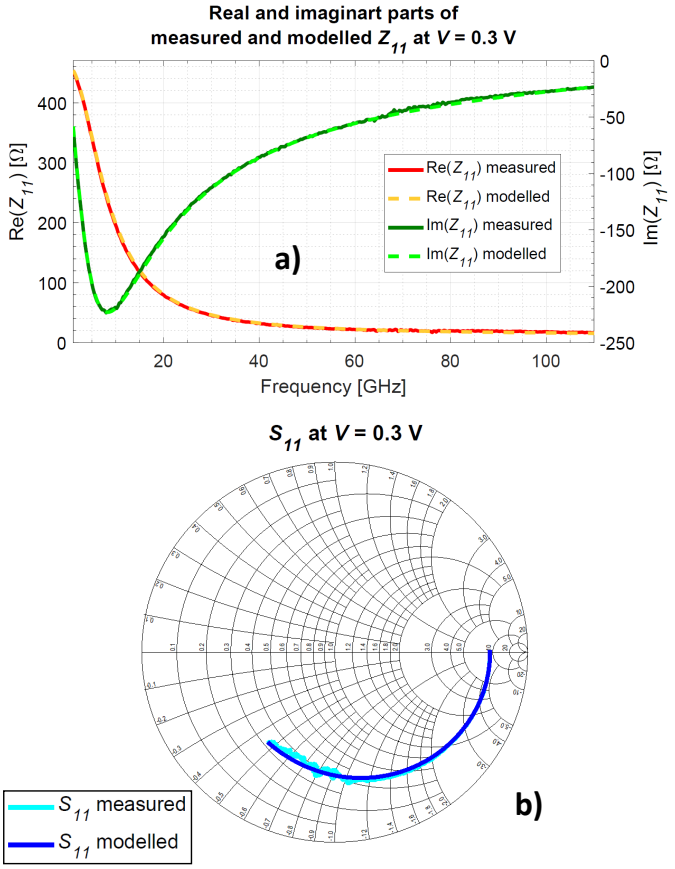

Fig. 3. In a), measured and modelled real and imaginary parts of Z_{11} at $V = 0.3$ V. In b), measured and modelled S_{11} at $V = 0.3$ V.

Table 2. RTD device and bond-pad small-signal parameters at V = 2.7 V

C_p [fF]	L_p [pH]	R_s [Ω]	G_{rtd} [mS]	C_{rtd} [fF]	L_{qw} [pH]
17	21	42.1	2.4	27.3	130

In the above, C_p and L_p model the bond-pads parasitic capacitance and inductance, respectively.

was employed. Further details on the extraction procedure were reported in [6]. The heterostructure features a cut-off frequency $f_c \simeq 534$ GHz and an RF power $P_{RF} \simeq 0.20$ mW/μm^2 at 300 GHz. More details can be found in [6]. Assuming a shunt resistance $R_{st} = 10$ Ω, the maximum device area $A_{max} = 2\Delta V/3\Delta J R_{st}$ is ~ 58 μm^2 from low-frequency stabilisation criteria [3]. Therefore, 25 μm^2, 36 μm^2, and 49 μm^2 large RTD devices can be expected to deliver up to $\simeq 5$ mW, $\simeq 7$ mW, and $\simeq 10$ mW of RF power at 300 GHz, respectively. For the estimation, a specific contact resistivity $\rho_c = 4$ Ω μm^2 was assumed, which was extracted through transfer length model (TLM) measurements of molybdenum (Mo)-based Ohmic contacts (Mo/Ti/Au), as shown in Fig. 4. The fabrication of the TLM structures included a pre-evaporation de-oxidation cleaning procedure consisting of a 64.5 min UV/O_3 exposure followed by a 2 min wet etch in a hydrochloric acid-based solution (HCl:H_2O=1:3) and a 40 s-long argon (Ar^+)-based ion milling. The deposition chamber loading time was kept around 30 s. Further details on the design and fabrication of the employed TLM structure can be found in [7].

III. RF STUBS DESIGN

Two different shorted transmission line inductive stubs were designed to be employed as LC tank component in practical RTD oscillator circuits operating at 300 GHz [1]. The first consisted of a CPW line with low characteristic impedance $Z_0 = 26$ Ω and relative effective permittivity $\epsilon_{r,eff} \simeq 6.4$, featuring signal line width $w = 46$ μm and short gap width $g = 3$ μm to correctly support the associated quasi-TEM mode at high-frequency. The second consisted of a microstrip line (MLIN) with low $Z_0 = 10$ Ω and $\epsilon_{r,eff} \simeq 3.2$, featuring $w = 21$ μm and a

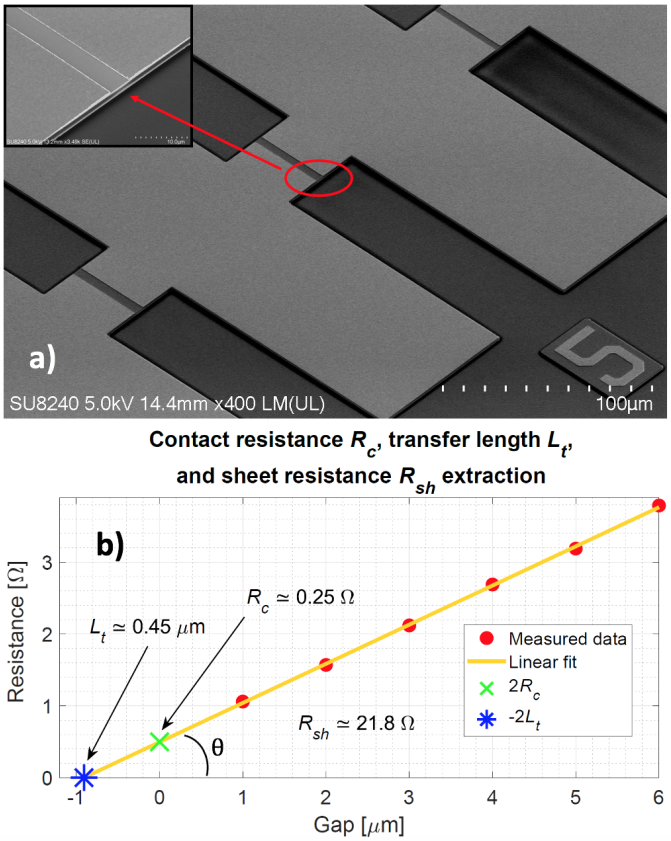

Fig. 4. In a), SEM image of an employed TLM structure for the extraction of ρ_c, featuring gap spacing ranging from 1 μm to 6 μm, together with a zoom-in over the 5 μm-wide gap. In b), extraction of contact resistance R_c, transfer length L_t, and sheet resistance $R_{sh} \propto tan\theta$.

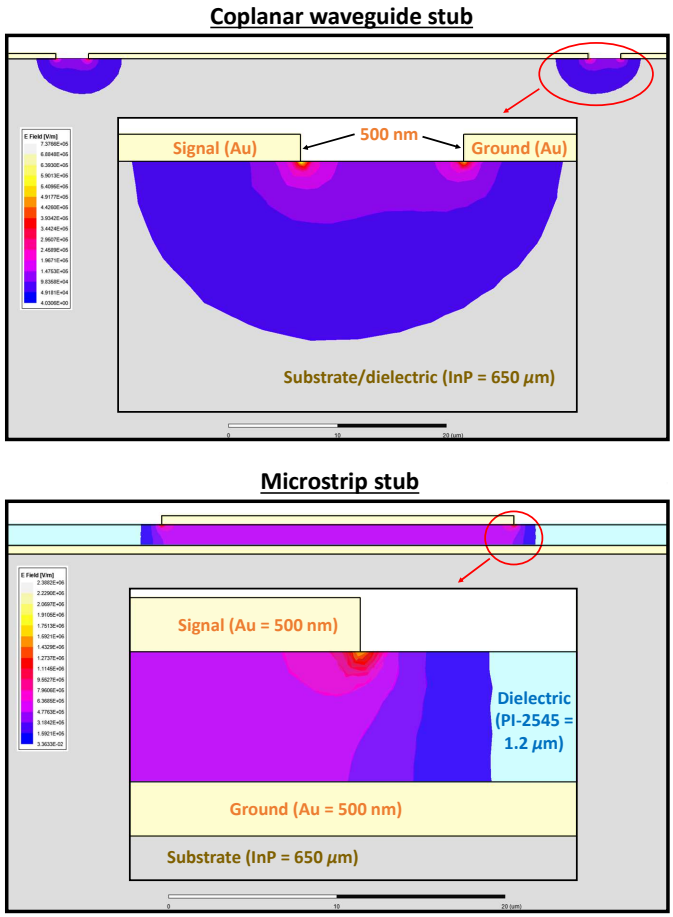

Fig. 5. Cross section of simulated 5 μm-long 26 Ω CPW and 20 μm-long 10 Ω MLIN stubs, showing the associated quasi-TEM standing wave 2D electric field magnitude E_{xy} at 300 GHz in proximity to a reference node.

1.2 μm-thick polyimide PI-2545-based dielectric layer with relative permittivity $\epsilon_r = 3.5$. The stubs were designed in ADS employing approximate quasi-static analytical models and then investigated in Ansys HFSS through full FEM-based 3D high-frequency electromagnetic numerical simulations, accurately accounting for both conductor/dielectric losses and frequency dispersion. Both structures were simulated on top of 650 μm-thick InP substrates with $\epsilon_r \simeq 12.5$ assuming Au-based signal/ground lines of thickness $t = 500$ nm (with $t > 3\delta$ for low signal attenuation, being $\delta \simeq 144$ nm the skin depth at 300 GHz) and ground lines width $s > 5w/2$ to ensure minimal radiation losses. From a circuit design perspective, the lines are shorted by 75 nm-thick silicon nitride (Si_3N_4, $\epsilon_r \simeq 6.8$) metal-insulator-metal (MIM) capacitors, which are designed to act as low impedance paths at the oscillation frequency, decoupling the RF part of the circuit from the DC bias supply [3]. Fig. 5 shows an example of simulated stub in both the adopted CPW and MLIN topologies at 300 GHz.

In the lossless limit, the stub shows inductive behaviour when its purely imaginary input impedance $Z_{in} = jZ_0 tan(\beta l) > 0$, i.e., $m\pi/2 < \beta l < n\pi/2$, being βl the line phase length, l the length of the stub, and $\beta \propto f\sqrt{\epsilon_{r,eff}}$ (assuming perfect TEM operation) the imaginary part of the propagation constant (being f the operation frequency), while m and n are positive whole even and positive odd integers, respectively. This approximately turns in $0 < l < 98$ μm and $0 < l < 139$ μm for short ($\beta l < \pi/2$) adopted CPW and MLIN designs operating at 300 GHz, respectively. Fig. 6 shows an example of simulated S_{11} parameter of a CPW and MLIN stubs in the frequency range 250−350 GHz, confirming the inductive nature of the lines. The average insertion loss *IL* was estimated to be $\simeq 8.5\times10^{-3}$ dB/μm and $\simeq 5.2\times10^{-3}$ dB/μm at 300 GHz for the CPW and MLIN geometries, respectively, from the simulated S_{21} parameter. Fig. 7 shows the simulated inductance $L = \text{Im}(Z_{11})/2\pi f$ of both CPW and MLIN stubs at 300 GHz, resulting in average linear densities of $\simeq 0.33$ pH/μm and $\simeq 0.07$ pH/μm, respectively.

The oscillation frequency can be approximated as [1]:

$$f_{osc} \approx \frac{\sqrt{L - C_{rtd}R_s^2}}{2\pi L\sqrt{C_{rtd}}(1 + R_s G_L)} \quad (1)$$

where G_L is the load conductance and $R_s \approx R_c \approx \rho_c A$, being R_c the parasitic Ohmic contact resistance and A the RTD top mesa area [6], from which $L > L_{min} \approx C_{rtd}R_c^2$ for the circuit to oscillate. Table 3 reports the parameters for 300-GHz oscillations. Clearly, the CPW implementation requires gap spacing of 3 μm and ultra-short line lengths

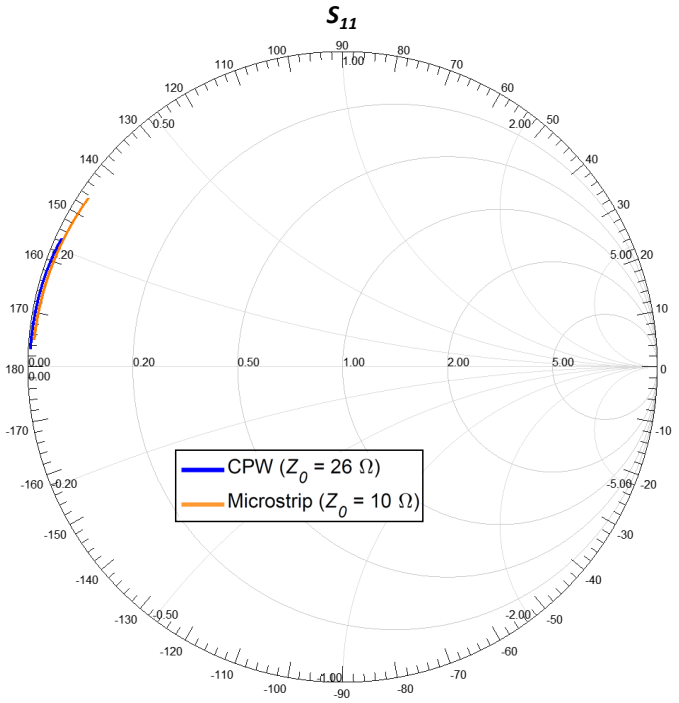

Fig. 6. Simulated S_{11} parameter of 5 μm-long 26 Ω CPW and 20 μm-long 10 Ω MLIN stubs in the frequency range 250−350 GHz.

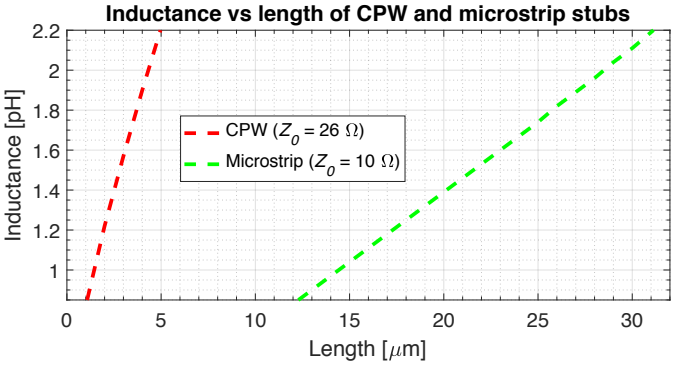

Fig. 7. Simulated inductance versus length of the analysed 26 Ω CPW and 10 Ω MLIN stubs at 300 GHz.

down to 1 μm, approaching the optical lithographic resolution limit and resulting in fabrication issues in terms of both mask alignment and reliable lift-off. On the other hand, the MLIN design allows for longer lines well above 10 μm due to the lower inductance density, however, at the expense of higher signal losses.

IV. Conclusions

We designed and experimentally investigated an InP RTD heterostructure for low-THz emitters, revealing an expected RF power performance of up to around 10 mW at 300 GHz. Coplanar and microstrip inductive stubs for practical oscillator circuit realisation employing low-cost photolithography were analysed through full electromagnetic simulations. Future work will consist in designing and fabricating oscillator sources based on the reported or similar epitaxial structures.

Table 3. 300-GHz (fundamental) oscillations parameters

A	25 μm^2	36 μm^2	49 μm^2
R_c	0.16 Ω	0.11 Ω	0.08 Ω
C_{rtd}	146.3 fF	210.6 fF	286.7 fF
L_{min}	3.7 fH	2.6 fH	1.9 fH
L(300 GHz)*	1.90 pH	1.32 pH	0.97 pH
l(CPW)	4 μm	2 μm	1 μm
IL(CPW)	0.034 dB	0.017 dB	0.008 dB
l(MLIN)	27 μm	19 μm	14 μm
IL(MLIN)	0.140 dB	0.099 dB	0.073 dB

* Computed assuming a standard 50 Ω load (G_L = 20 mS).

V. Acknowledgments

The authors would like to thank the James Watt Nanofabrication Centre (JWNC) staff, University of Glasgow, for the support during devices fabrication.

The work of Davide Cimbri was supported by TeraApps (Doctoral Training Network in Terahertz Technologies for Imaging, Radar and Communication Applications), which received funding from the European Union's Horizon 2020 research and innovation programme under Marie Skłodowska-Curie Innovative Training Network (ITN) grant agreement No. 765426.

References

[1] D. Cimbri, J. Wang, A. Al-Khalidi, and E. Wasige, "Resonant Tunnelling Diode High-Speed Terahartz Wireless Communications - A Review," *IEEE Transactions on Terahertz Science and Technology*, vol. 12, no. 3, pp. 226-244, 2022, doi: 10.1109/TTHZ.2022.3142965.

[2] J. Wang, M. Naftaly, and E. Wasige, "An Overview of Terahertz Imaging with Resonant Tunneling Diodes," *Applied Sciences*, vol. 12, no. 8, pp. 3822, 2022, doi: 10.3390/app12083822.

[3] A. Al-Khalidi, K. H. Alharbi, J. Wang, R. Morariu, L. Wang, A. Khalid, J. M. L. Figueiredo, and E. Wasige, "Resonant Tunneling Diode Terahertz Sources With up to 1 mW Output Power in the J-Band," *IEEE Transactions on Terahertz Science and Technology*, vol. 10, no. 2, pp. 150-157, 2020, doi: 10.1109/TTHZ.2019.2959210.

[4] D. Cimbri, B. Yavas-Aydin, F. Hartmann, F. Jabeen, L. Worschech, S. Höfling, and E. Wasige, "Accurate Quantum Transport Modelling of High-Speed $In_{0.53}Ga_{0.47}As$/AlAs Double-Barrier Resonant Tunnelling Diodes," *IEEE Transactions on Electron Devices*, 2022, doi: 10.1109/TED.2022.3178360.

[5] D. Cimbri, J. Wang, and E. Wasige, "Epitaxial Structure Simulation Study of $In_{0.53}Ga_{0.47}As$/AlAs Double-Barrier Resonant Tunnelling Diodes," *2022 Fifth IEEE International Workshop on Mobile Terahertz Systems (IWMTS)*, Duisburg-Essen, 4-6th July 2022.

[6] D. Cimbri, R. Morariu, A. Ofiare, and E. Wasige, "$In_{0.53}Ga_{0.47}As$/AlAs Double-Barrier Resonant Tunnelling Diodes with High-Power Performance in the Low-Terahertz Band," *2022 Fifth IEEE International Workshop on Mobile Terahertz Systems (IWMTS)*, Duisburg-Essen, 4-6th July 2022.

[7] D. Cimbri, N. Weimann, Q. R. A. Al-Taai, A. Ofiare, and E. Wasige, "Ohmic Contacts Optimisation for High-Power InGaAs/AlAs Double-Barrier Resonant Tunnelling Diodes Based on a Dual-Exposure E-Beam Lithography Approach," *International Journal of Nanoelectronics and Materials*, vol. 14 (Special Issue), pp. 11-19, 2021.